

Ultracompact and Unidirectional On-Chip Light Source Based on Epsilon-Near-Zero Materials in an Optical Communication Range

You Wu,¹ Xiaoyong Hu,^{1,2,3,*} Feifan Wang,¹ Jinghuan Yang,¹ Cuicui Lu,^{4,†} Yong-Chun Liu,⁵ Hong Yang,^{1,2} and Qihuang Gong^{1,2,3}

¹*State Key Laboratory for Mesoscopic Physics & Department of Physics, Collaborative Innovation Center of Quantum Matter, Nano-optoelectronics Frontier Center of Ministry of Education, Peking University, Beijing 100871, China*

²*Collaborative Innovation Center of Extreme Optics, Shanxi University, Taiyuan, Shanxi 030006, China*

³*Beijing Academy of Quantum Information Sciences, Beijing 100193, China*

⁴*Beijing Key Laboratory of Nanophotonics and Ultrafine Optoelectronic Systems, School of Physics, Beijing Institute of Technology, Beijing 100081, China*

⁵*State Key Laboratory of Low-Dimensional Quantum Physics, Department of Physics, Collaborative Innovation Center of Quantum Matter, Tsinghua University, Beijing 100084, China*



(Received 19 November 2017; revised manuscript received 4 October 2019; published 8 November 2019)

An on-chip light source is one of the essential components for integrated photonic circuits and quantum-information processing chips. To date, it has been a great challenge to construct an on-chip light source with high directionality, high collection efficiency, and ultrasmall feature size simultaneously in the optical communication range. Here, an on-chip light source, consisting of a circular paraboloid etched in an aluminum-doped zinc-oxide film, which is an epsilon-near-zero material, is experimentally realized at 1550 nm. Photons emitted from the a PbS quantum-dot cluster placed near the focal point of this paraboloid are reflected into a directional parallel beam due to the large impedance mismatch between aluminum-doped zinc oxide and ambient medium. An ultrasmall emission divergence angle of only $\pm 3^\circ$, and an ultrahigh directional emission contrast ratio of 44 dB are achieved from the ultracompact device with a feature size of only $1.5 \mu\text{m}$. Also, an ultrahigh collection efficiency of up to 92% is predicted by simulation. This work not only opens an alternative way for the realization of integrated photonic devices based on epsilon-near-zero materials, but also provides another method for the precise assembling of composite functional nanostructures.

DOI: 10.1103/PhysRevApplied.12.054021

I. INTRODUCTION

On-chip light sources are important elementary components for integrated photonic circuits. The compactness of light sources can immensely improve the integration density [1–3]. For an ideal on-chip light source, ultracompact feature size, ultrahigh directionality, and collection efficiency are the most significant indexes. Several schemes are proposed to improve these indexes, such as using surface plasmons [4] and hybrid plasmon nanostructures [5,6]. However, large propagation losses of surface plasmons and multiple transformation process in hybrid plasmon nanostructures decreased the collection efficiency. Photonic microstructures had the potential of realizing unidirectional emission of emitters. Photonic crystal structures [7–9], metamaterial cavities [10], nanobeam waveguides [11], and pillar microcavities [12]

could effectively control the emission directivity. However, some of these photonic microstructures had a feature size of several hundreds of micrometers, and it is difficult to collect the photons emitted out of these structures, while some other microstructures need external magnetic field to separate photons with different polarizations, which limits the integration with other photonic devices. The light sources with quantum emitters embedded in tapered photonic waveguides are much easier for integration, while the collection efficiency is limited [13–16]. Moreover, previously reported on-chip light sources mainly focused on the operating wavelength within the visible range or around 800 nm. In the optical communication range, quantum dots such as PbS [17], InAs [18], and (In,As)P [13] can emit photons around 1550 nm. However, different from semiconductor quantum dots, which are usually epitaxial grown and embedded in another semiconductor bulk material [19], PbS quantum dots are easily synthesized by wet chemistry techniques, so that a single quantum dot can exist in the suspension. Therefore, PbS quantum dots

*xiaoyonghu@pku.edu.cn

†cuicuilu@bit.edu.cn

are promising in constructing composite nanostructures at optical communication range, since a single quantum dot or cluster is compatible with precise nanomanipulation techniques [20]. However, due to the technical challenges of manipulating quantum dots in nanoscale, there is no report on unidirectional light sources based on PbS quantum dots, as far as we know. To date, it is still a great challenge to realize an on-chip light source with high directionality, high collection efficiency, and ultrasmall feature size simultaneously in the optical communication range.

Here, we report the realization of an ultracompact on-chip light source with ultrahigh directionality and collection efficiency simultaneously in the optical communication range. The on-chip light source is composed of a circular paraboloid etched in aluminum-doped zinc-oxide (Al:ZnO, AZO) film, which is an epsilon-near-zero (ENZ) material, with PbS quantum dot cluster placed near the focal point of this circular paraboloid. The dielectric function of the ENZ material is $\varepsilon = \varepsilon_1 - i\varepsilon_2$, where ε_1 and ε_2 are the real and imaginary parts, respectively. At the ENZ frequency ($\varepsilon_1 \approx 0$), the amplitude and the phase of electromagnetic waves can be prominently controlled [21]. Therefore, ENZ materials have been applied to shape the radiation pattern of a source [10,22–24], or to construct light-transmission waveguide devices [25], all-optical switchings [26,27], frequency variation devices [28], and so on. Recently, it is reported that AZO's permittivity crossed zero around the 1550-nm wavelength with relatively low intrinsic losses [26,29–31]. In this paper, we propose the use of large impedance mismatch at the boundary of AZO and free space to reflect photons, which would further reduce the influence of AZO's losses, since electromagnetic waves do not propagate through the AZO material. The photons emitted can be directly coupled to a waveguide with the maximum collection efficiency of 92% according to the simulation. Compared with the same structures built on a gold or silver film, the collection efficiency is higher (see Table S1 in the Supplemental Material [32]). The overall performance of this light source is also superior to that of the bullseye grating [33,34] and micropillar structures [12,35,36], while the device footprint is much smaller. Moreover, we creatively develop a nanomanipulation method of fabricating composite nanostructures through precisely manipulating 200-nm-sized particles to a target nanostructure, by using a SEM equipped with a nanomanipulator. We demonstrate the manipulation of PbS quantum dots with high precision of several nanometers by using the nanomanipulation method to fabricate our on-chip light-source sample. The introduction of the nanomanipulator overcomes the fabrication challenge for structures composed of nanostructures and quantum dots or other nanoparticles [20], which proposes a new way for the realization of composite nanostructures and photonic devices.

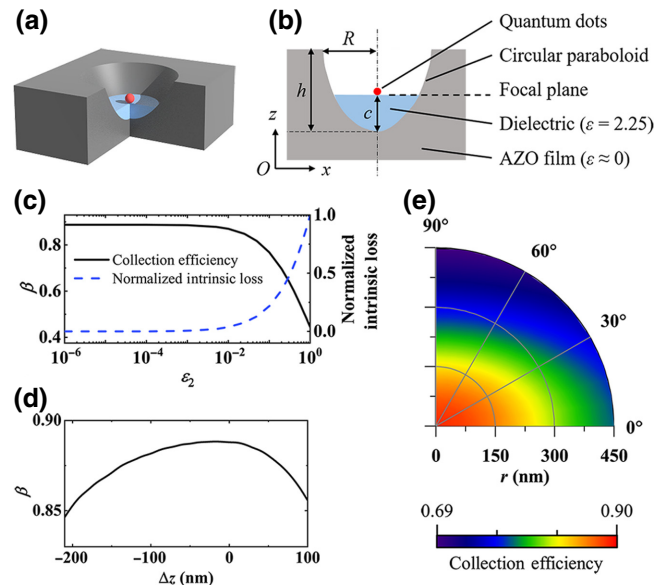


FIG. 1. Three-dimensional illustration (a) and the z - x cross section (b) of the designed rotational symmetric structure. The substrate is an ENZ circular paraboloid (AZO film). Quantum dots are located near the focal point of the circular paraboloid on a layer of dielectric ($\varepsilon = 2.25$). $R = 780$ nm, $h = 650$ nm, and $c = 234$ nm. (c) The collection efficiency (black solid line) and intrinsic loss (blue dashed line) in the ENZ medium (normalized to the intrinsic loss when $\varepsilon_2 = 1$) when ε_2 increases from 10^{-6} to 1. (d) Collection efficiency remains high when the quantum dots deviate from the focal point in the z direction. (e) Collection efficiency decreases gradually when the quantum dots are off center. Because the polarization of the dipole in our simulation is along the x direction, the figure is not perfectly symmetric.

II. DESIGN AND SIMULATIONS

A three-dimensional illustration and the cross section of the structure are shown in Figs. 1(a) and 1(b).

A circular paraboloid is etched in the AZO film ($\varepsilon \approx -0.5 i$ at 1550 nm), with the depth of 650 nm and the aperture radius of 780 nm. This means that the on-chip light source has an ultrasmall feature size of about $1.5 \mu\text{m}$, which is only one wavelength order. The PbS quantum-dot clusters are placed near the focal point of this circular paraboloid on a layer of SiO_2 by using the nanomanipulation method. The designed circular paraboloid structure plays the role of a reflector, where photons emitted from the PbS quantum dots located at the focal point are reflected into a parallel beam. The high reflectivity can be understood as a result of impedance mismatching. The wave impedance of an electromagnetic wave is defined as

$$Z = \sqrt{\mu/\varepsilon}, \quad (1)$$

where μ and ε are permeability and permittivity, respectively. For the free space, $Z_0 \approx 377\Omega$, while for an ENZ medium ($\varepsilon \approx 0$), the impedance approaches infinity.

Therefore, large impedance mismatch occurs at the interface between ENZ material and ordinary medium, leading to very high reflectivity. Such a process can also be intuitively understood by the Snell-Decartes law, which is also known as the law of refraction. Since the refractive index of ENZ material, $n_{\text{ENZ}} = \sqrt{\epsilon}$, is far smaller than that of the ordinary medium, the critical angle

$$\theta_C = \arcsin \frac{n_{\text{ENZ}}}{n_m}, \quad (2)$$

is close to zero, where n_m is the refractive index of the ordinary medium (such as air or SiO_2 here). Owing to the mechanism of total internal reflection, photons emitted from the quantum emitter located at the focal point are reflected when they arrive at the boundary. Moreover, since the physical mechanism here has nothing to do with the resonance of the structure or the wavelength of the quantum dots, this unidirectional light source is expected to enable a broad bandwidth.

The three-dimensional simulations are based on the finite-element method with COMSOL Multiphysics software. The quantum emitter is considered as an oscillating classical point dipole [5], and model setup details are presented in the Supplemental Material [32]. In consideration of the cascaded connection of such a unidirectional light source with subsequent photonic information processing units, we calculate the collection efficiency when a waveguide is connected (see Fig. S1 in Supplemental Material [32] for the details). The collection efficiency is an important figure of merit for an integrated light source, which defines the coupling efficiency of emitted photons to a waveguide mode [8]:

$$\beta = \frac{\gamma_{\text{wg}}}{\gamma_{\text{total}}} = \frac{\gamma_{\text{wg}}}{\gamma_{\text{wg}} + \gamma_{\text{farfield}} + \gamma_{\text{nonrad}}}, \quad (3)$$

where γ_{total} , γ_{wg} , and γ_{farfield} are the total decay rates and those coupled to the waveguide channel or radiated to the far field, respectively, and γ_{nonrad} is the intrinsic nonradiative decay rate of the quantum dots, which is neglected in our calculations. The collection efficiency at the wavelength of 1550 nm could reach 89% when the thickness of AZO film is 900 nm. In fact, the collection efficiency could reach up to 92% by tuning the thickness of AZO. The rest energy is leaked to the free space and the substrate. This means that the photons unidirectionally emitted from this on-chip light source can be efficiently collected and coupled to a waveguide with an ultrahigh efficiency of 89%.

In order to better improve the device properties, we further analyzed the influence factors. There are several factors that could influence the light source's performance, including the losses of the AZO film and the inaccuracy of the sample fabrication. Considering the different losses in practical AZO materials, we calculate collection efficiency

with a different imaginary part of permittivity ϵ_2 using the finite-element method, as shown in Fig. 1(c). The collection efficiency slightly decreased from 89 to 77% when ϵ_2 increased from 10^{-6} to 0.1, which is a general variation range for the ENZ materials. This reduced part of photons collected is a result of incremental intrinsic losses in the AZO film [blue dashed line in Fig. 1(c)]. The larger ϵ_2 leads to a significant increase in the intrinsic losses. Here, the intrinsic losses are normalized to that when $\epsilon_2 = 1$. Another non-negligible error that will be introduced in real experiments is the position deviation of the quantum dots, which is limited by the manipulating precision. For evaluation of the influence, we first assume the quantum dots are located along the axis of symmetry, while the z coordinate varied [Fig. 1(d)]. In fact, the collection efficiency maintained the maximum of about 89% when the quantum emitter is around the focal plane in a relatively large range of about 90 nm ($-70 \text{ nm} \leq \Delta z \leq 20 \text{ nm}$, where Δz denotes the deviation of the quantum dots from the focal point in the z direction). Even when Δz increases to 100 nm, the collection efficiency is still as large as 86%, which means the performance is not sensitive to the deviation of the quantum dots' position in the z direction. In the experiment, the z coordinate of the quantum dots is decided by the thickness of the dielectric layer, which could be precisely controlled in the deposition process, as we discuss below, while the horizontal position is relatively more difficult to control. Supposing $\Delta z = 0$ here, the collection efficiency declines gradually with the increase of radial coordinate r [Fig. 1(e)]. Note that the dipole moment is along the direction in our simulations, therefore the collection efficiency is different for different azimuth angles. However, even with a considerable deviation of 450 nm from the focal point, the collection efficiency could still reach 70%. In the Supplemental Material (Fig. S2) [32], we also present the calculated far-field patterns when introducing such a deviation of the quantum dots' position. The results indicated that the far-field pattern is almost unchanged with different Δz from -70 to 100 nm, and would be rotated with the pattern shape almost unchanged when r increased. The above simulation results indicate that some imperfections in experiments are acceptable and do not seriously influence the properties of the device.

III. EXPERIMENTAL MEASUREMENTS

In the experiment, we use colloidal PbS quantum dots (Mesolight, PbS-1550-50) as quantum emitters. The emission peak of PbS quantum dots is around 1550 nm (see Supplemental Material [32]). The absorption peak of PbS quantum dots is about 350 nm. The sample fabrication process is shown in Fig. 2(a). We develop a nanomanipulation method to fabricate composite nanostructures by introducing the nanomanipulators (Oxford Instruments, OmniProbe 100 and OmniProbe 400) into the focused

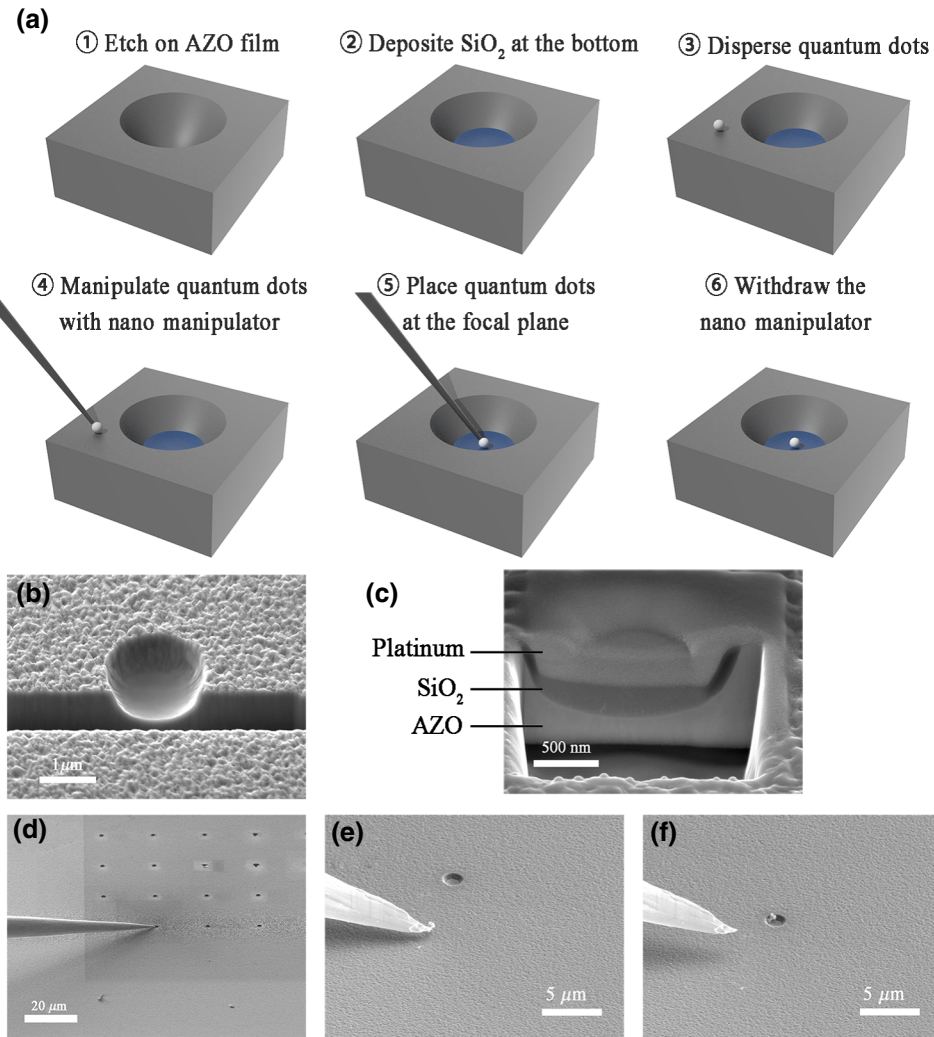
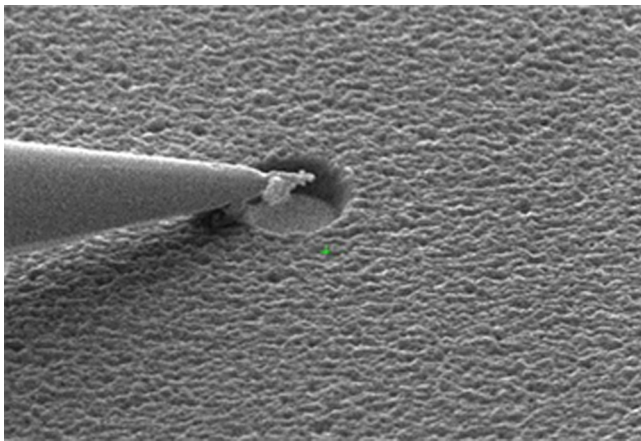


FIG. 2. Sample fabrication process and SEM images. (a) The fabrication process. (b) SEM image of the cross section of a paraboloid hole. (c) SEM image after depositing SiO_2 layer, where the platinum is deposited for the protection of SiO_2 and AZO while etching with FIB in order to view the thickness of SiO_2 . For the practical samples, there are no platinum. (d) SEM image when the nanomanipulator's tip is touching the sample surface. (e) SEM image of a cluster of quantum dots attaching on the tip. (f) SEM image after the quantum dots are placed at the SiO_2 base plane.

ion beam(FIB) systems (ZEISS Crossbeam 540 and FEI Helios NanoLab 600i FIB/SEM DualBeam Microscopes). The detailed fabrication condition and SEM images can be found in the Supplemental Material [32]. The fabrication process included six steps: (1) etching circular paraboloid holes in the AZO film with FIB; (2) depositing the SiO_2 layer at the bottom of the holes with gas-injection system in order to provide a base plane in the paraboloid for the quantum dots; (3) dispersing the PbS quantum dots on the surface of AZO film by spin-coating method; (4) grinding and polishing tungsten tip, and manipulating quantum dots with the nanomanipulator; (5) placing quantum dots at the base plane in the hole; (6) withdrawing the nanomanipulator. Figure 2(b) is the cross section of an etched circular paraboloid on the AZO film. A layer of SiO_2 is deposited precisely at the bottom of the paraboloid. A cross section is shown in Fig. 2(c), where the platinum is deposited for the protection of SiO_2 and AZO underneath when etching the cross section with FIB. This could help to measure the thickness of SiO_2 in order to determine the proper fabricating parameters. The next step is the most

challenging when preparing the sample, where a tungsten tip is adopted to manipulate the quantum dots. The size of a single PbS quantum dot is about 10–15 nm, while the clusters of PbS quantum dots sized about 200 nm can be obtained after spin coating the methylbenzene-solution-doped PbS quantum dots, the size of which is a benefit for our nanomanipulation. The tip of the nanomanipulator is further polished with FIB, and the tip size could be several tens of nanometers, comparable to PbS quantum-dot clusters. Figure 2(d) shows a perspective SEM image when a nanomanipulator is touching the sample surface. With this self-made tip, we manage to move a cluster of quantum dots to the SiO_2 base plane and withdrew the nanomanipulator, as shown in Figs. 2(e) and 2(f). A video record of our operation under SEM is presented in Video 1.

We perform measurement of the far-field emission pattern from this light source in a system shown in Fig. 3(a). A 12 \times zoom lens system is used to find the structure, where a 10 \times objective helped to get a larger magnification. A visible light CCD is coupled to the system, which can directly display the image of the sample surface on the screen.



VIDEO 1. A video record about the manipulation of quantum dots with the nanomanipulator under SEM.

After identifying a structure, the excitation of quantum dots is through a 405-nm semiconductor continuous-wave laser (CNI, MDL-III-405). The violet laser is reflected by a long-pass dichroic mirror. A 100 \times objective (Mitutoyo, M Plan Apo NIR HR 100 \times , N.A. = 0.7) is used to focus the exciting laser at the target region on the sample. Therefore, photons would emit from the excited quantum dots and be collected by the 100 \times objective again. These near-infrared photons can propagate through the dichroic mirror with high transmittance. In order to detect such a weak signal, a fiber collimator is applied to improve the coupling efficiency of photons into the fiber. The measurement is accomplished by a single photon detector (QASKY, WT-SPD300-ULN), whose detection range covers 950–1650 nm. Therefore, the emitted infrared signals from the PbS quantum dots could be detected with high efficiency, while the exciting laser had no contributions to the photon counting. In order to measure the photon-emission signals at different directions, the sample is installed on a rotation stage and coupled to a three-dimensional positioning system. Figure 3(b) shows the top view of the sample and the optical path. In the experiment, the power of the exciting laser is 0.885 mW near the sample surface.

The measured far-field radiation pattern is shown in Fig. 3(c), which distinctly illustrates unidirectional photon emission from this structure normal to the sample surface. The emission of photons is mainly located at 90° with a FWHM divergence of $\pm 3^\circ$ in the experiment. Such an ultrasmall emission divergence angle ensures an ultrahigh directionality of the on-chip light source. We also perform simulations to show the energy density distribution at the cross section of the designed three-dimensional model, which is presented in the inset of Fig. 3(b). The contrast ratio between the energy above and below the ENZ film is as large as 44 dB, which also proves that the light source is highly unidirectional, almost without backward emission

loss. The green and red curves in Fig. 3(c) are the simulated far-field patterns. The former is when the quantum dot is put on an unstructured AZO film, and the divergence angle is up to $\pm 41^\circ$. The latter is the result when the quantum dot is well located inside the nanostructure. The FWHM divergence of the photon emission is $\pm 12^\circ$ according to the simulation, also indicating the unidirectional emission of photons in this device. The directivity of emission, which is defined as the ratio of the maximum emission intensity to the average intensity in 4π solid angle [37], is 15.1 and 13.2 in the experiment and the simulation, respectively. Note that the performance of the device in our experiment is even superior to simulation results. This can be possibly attributed to the following reasons. First, in the simulation the quantum emitter is a dipole parallel to the plane, and the direction of dipole moment may have influences on the performance. However, in the experiment a cluster of quantum dots emitted photons together, the superposition may enhance the directional property. Second, the algorithm of simulation software probably differs from real measurements, where the detection sensitivity is limited for weak signals. The photon emission from the light source we design is highly unidirectional, so that the emission to the other directions except the vertical direction is very weak. The photon counts in these directions dropped quickly when the detection angle is away from vertical, and would be submerged by noise.

The experimental results above demonstrate that this unidirectional light source has superior performance at the wavelength of 1550 nm. Actually this light source supported a wide bandwidth, which covered the emission spectrum of the PbS quantum dots. We further consider the actual material dispersion of AZO [31], and find that this unidirectional light source can work at a wide bandwidth with high performance. Figure 4(a) shows the far-field light distribution pattern at the wavelengths from 1400 to 1700 nm. In a bandwidth range of 100 nm (from 1500 to 1600 nm), which covered the emission peak of PbS quantum dots, the far-field light-distribution pattern is almost unchanged. Furthermore, this designed circular paraboloid nanostructure can be applied to construct light sources in a broader bandwidth, including the visible light range. As shown in Fig. 4(b), assuming proper ENZ materials at different wavelengths can be obtained (e.g., transparent conduction oxides [29] and artificial metamaterials [38]), we chose six different common quantum emitters (N-V⁰ center, N-V⁻ center [37], InP-(In, Ga)P [39], SiV center [40], InAs-GaAs-(In, Ga)As [41], and PbS). Here, the structure parameters are simply kept the same, while the emission peak of these quantum-emitter ranges from 575 to 1550 nm. Figure 4(b) shows the calculated collection efficiency and the contrast ratio. It can be found that collection efficiency is higher than 89% for each quantum emitter, and the maximum could even reach

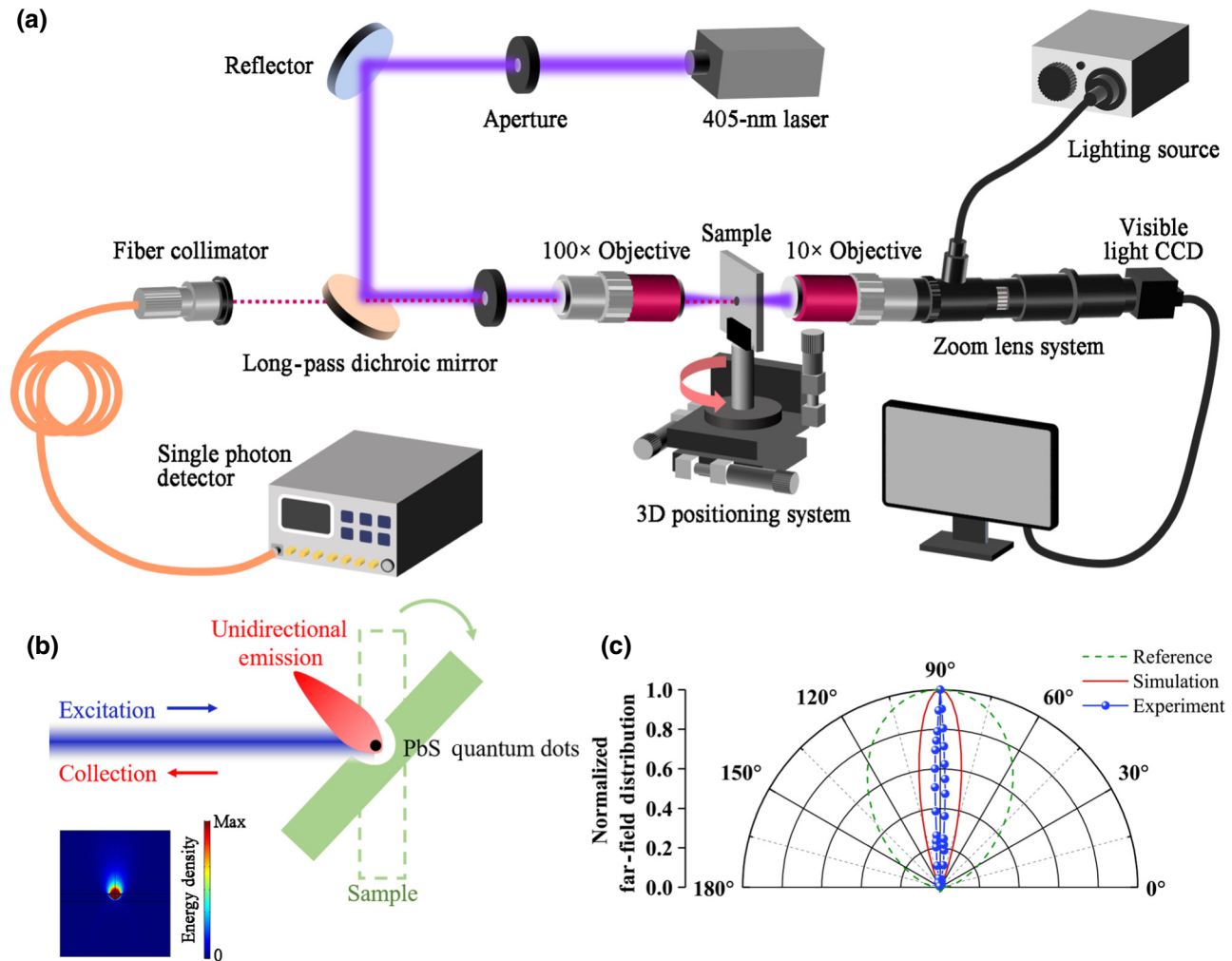


FIG. 3. (a) Experimental setup of the measurements. A zoom lens system with a visible light CCD is used to find and locate the target nanostructure. A 405-nm laser is focused on the sample surface to excite the quantum dots in the nanostructure. The emitted photons propagated through the dichroic mirror and are collected by a fiber collimator connected to a single photon detector. The sample is installed on a rotation stage and coupled to a three-dimensional positioning system, so that photons emitted to different directions can be collected, respectively. (b) The top view of the sample and the optical path. Inset: calculated energy density distribution at the cross section of the designed three-dimensional model. (c) Far-field light-distribution patterns from simulation (red) and experiment (blue). The far-field distribution when the quantum dot is put on an unstructured AZO film is also shown (green dotted curve). Background noise is subtracted from measured results.

99% for the $N-V^-$ center. The contrast ratio is always larger than 32 dB for different quantum emitters. Therefore, this designed circular paraboloid nanostructure performs well from the visible to near-infrared wavelengths, and can be expected to realize high-performance single-photon sources by choosing proper single quantum emitters.

IV. SUMMARY

In summary, an ultracompact on-chip light source with ultrahigh directionality and collection efficiency is realized in the optical communication range. A circular paraboloid

etched in aluminum-doped zinc-oxide film, with PbS quantum dots placed near the focal point, is used to construct the on-chip light-source sample. An ultrasmall emission divergence angle of only $\pm 3^\circ$ is achieved experimentally and an ultrahigh collection efficiency of up to 92% is predicted by simulation from the ultracompact on-chip light source with a feature size of $1.5 \mu\text{m}$. This unidirectional light source can maintain high performance in a broad bandwidth. This work not only opens a new way for the realization of integrated photonic devices based on epsilon-near-zero materials, but also provides an advanced method for the precise assembling of composite functional nanostructures.

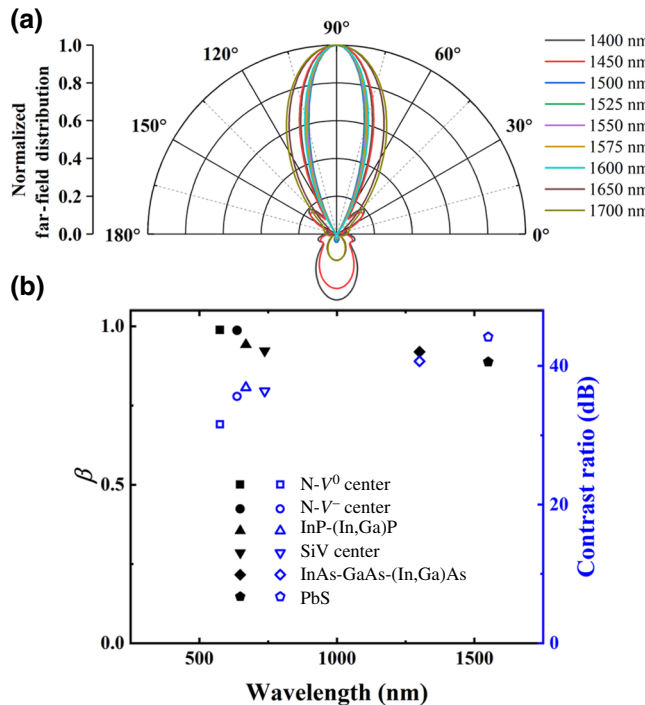


FIG. 4. (a) Simulated far-field emission pattern within the bandwidth of 300 nm, when taking the actual material dispersion into consideration [26]. (b) Collection efficiency and contrast ratio when adopting different quantum emitters and proper ENZ materials, assuming the structure parameters are the same as those in Fig. 1.

ACKNOWLEDGMENTS

This work is supported by the National Key Research and Development Program of China under Grant No. 2018YFB2200403, and the National Natural Science Foundation of China under Grants No. 61775003, No. 11734001, No. 91950204, No. 11527901, No. 91850111, No. 91850117, No. 11604378, No. 11654003, No. 11674390, and No. 91736106, and Beijing Municipal Science & Technology Commission Grant No. Z191100007219001.

- [1] Z. Zhou, B. Yin, and J. Michel, On-chip light sources for silicon photonics, *Light: Sci. Appl.* **4**, e358 (2015).
- [2] R. E. Camacho-Aguilera, Y. Cai, N. Patel, J. T. Bessette, M. Romagnoli, L. C. Kimerling, and J. Michel, An electrically pumped germanium laser, *Opt. Express* **20**, 11316 (2012).
- [3] X. Sun, A. Zadok, M. J. Shearn, K. A. Diest, A. Ghaffari, H. A. Atwater, A. Scherer, and A. Yariv, Electrically pumped hybrid evanescent Si/InGaAsP lasers, *Opt. Lett.* **34**, 1345 (2009).
- [4] A. V. Akimov, A. Mukherjee, C. L. Yu, D. E. Chang, A. S. Zibrov, P. R. Hemmer, H. Park, and M. D. Lukin,

- Generation of single optical plasmons in metallic nanowires coupled to quantum dots, *Nature* **450**, 402 (2007).
- [5] H. Lian, Y. Gu, J. Ren, F. Zhang, L. Wang, and Q. Gong, Efficient Single Photon Emission and Collection Based on Excitation of Gap Surface Plasmons, *Phys. Rev. Lett.* **114**, 193002 (2015).
 - [6] K. J. Russell, T. L. Liu, S. Y. Cui, and E. L. Hu, Large spontaneous emission enhancement in plasmonic nanocavities, *Nat. Photon.* **6**, 459 (2012).
 - [7] M. Toishi, D. Englund, A. Faraon, and J. Vuckovic, High-brightness single photon source from a quantum dot in a directional-emission nanocavity, *Opt. Express* **17**, 14618 (2009).
 - [8] M. Arcari, I. Söllner, A. Javadi, S. Lindskov Hansen, S. Mahmoodian, J. Liu, H. Thyrrstrup, E. H. Lee, J. D. Song, S. Stobbe, and P. Lodahl, Near-unity Coupling Efficiency of a Quantum Emitter to a Photonic Crystal Waveguide, *Phys. Rev. Lett.* **113**, 093603 (2014).
 - [9] I. Söllner, S. Mahmoodian, S. L. Hansen, L. Midolo, A. Javadi, G. Kirsanske, T. Pregnolato, H. El-Ella, E. H. Lee, J. D. Song, S. Stobbe, and P. Lodahl, Deterministic photon-emitter coupling in chiral photonic circuits, *Nat. Nanotechnol.* **10**, 775 (2015).
 - [10] J. Xu, G. Song, Z. Zhang, Y. Yang, H. Chen, M. S. Zubairy, and S. Zhu, Unidirectional single-photon generation via matched zero-index metamaterials, *Phys. Rev. B* **94**, 220103(R) (2016).
 - [11] R. J. Coles, D. M. Price, J. E. Dixon, B. Royall, E. Clarke, P. Kok, M. S. Skolnick, A. M. Fox, and M. N. Makhonin, Chirality of nanophotonic waveguide with embedded quantum emitter for unidirectional spin transfer, *Nat. Commun.* **7**, 11183 (2016).
 - [12] X. Ding, Y. He, Z.-C. Duan, N. Gregersen, M.-C. Chen, S. Unsleber, S. Maier, C. Schneider, M. Kamp, S. Höfling, C.-Y. Lu, and J.-W. Pan, On-demand Single Photons with High Extraction Efficiency and Near-unity Indistinguishability from a Resonantly Driven Quantum Dot in a Micropillar, *Phys. Rev. Lett.* **116**, 020401 (2016).
 - [13] S. Haffouz, K. D. Zeuner, D. Dalacu, P. J. Poole, J. Lapointe, D. Poitras, K. Mnaymneh, X. Wu, M. Couillard, M. Korkusinski, E. Scholl, K. D. Jons, V. Zwiller, and R. L. Williams, Bright single inasp quantum dots at telecom wavelengths in position-controlled inp nanowires: The role of the photonic waveguide, *Nano Lett.* **18**, 3047 (2018).
 - [14] M. E. Reimer, G. Bulgarini, N. Akopian, M. Hocevar, M. B. Bavinck, M. A. Verheijen, E. P. Bakkers, L. P. Kouwenhoven, and V. Zwiller, Bright single-photon sources in bottom-up tailored nanowires, *Nat. Commun.* **3**, 737 (2012).
 - [15] I. E. Zadeh, A. W. Elshaari, K. D. Jons, A. Fognini, D. Dalacu, P. J. Poole, M. E. Reimer, and V. Zwiller, Deterministic integration of single photon sources in silicon based photonic circuits, *Nano Lett.* **16**, 2289 (2016).
 - [16] J. Claudon, J. Bleuse, N. S. Malik, M. Bazin, P. Jaffrennou, N. Gregersen, C. Sauvan, P. Lalanne, and J.-M. Gérard, A highly efficient single-photon source based on a quantum dot in a photonic nanowire, *Nat. Photon.* **4**, 174 (2010).
 - [17] I. Moreels, Y. Justo, B. De Geyter, K. Hastraeete, J. C. Martins, and Z. Hens, Size-tunable, bright, and stable pbs quantum dots: A surface chemistry study, *ACS Nano* **5**, 2004 (2011).

- [18] S. Anantathanasarn, R. Nötzel, P. J. van Veldhoven, T. J. Eijkemans, and J. H. Wolter, Wavelength-tunable ($1.55\text{ }\mu\text{m}$ region) inas quantum dots in InGaAsP/InP (100) grown by metal-organic vapor-phase epitaxy, *J. Appl. Phys.* **98**, 013503 (2005).
- [19] P. Senellart, G. Solomon, and A. White, High-performance semiconductor quantum-dot single-photon sources, *Nat. Nanotechnol.* **12**, 1026 (2017).
- [20] E. Ampem-Lassen, D. A. Simpson, B. C. Gibson, S. Trpkovski, F. M. Hossain, S. T. Huntington, K. Ganesan, L. C. L. Hollenberg, and S. Prawer, Nano-manipulation of diamond-based single photon sources, *Opt. Express* **17**, 11287 (2009).
- [21] X. Niu, X. Hu, S. Chu, and Q. Gong, Epsilon-near-zero photonics: A new platform for integrated devices, *Adv. Opt. Mater.* **6**, 1701292 (2018).
- [22] A. Alù, M. G. Silveirinha, A. Salandrino, and N. Engheta, Epsilon-near-zero metamaterials and electromagnetic sources: Tailoring the radiation phase pattern, *Phys. Rev. B* **75**, 155410 (2007).
- [23] S. Enoch, G. Tayeb, P. Sabouroux, N. Guerin, and P. Vincent, A Metamaterial for Directive Emission, *Phys. Rev. Lett.* **89**, 213902 (2002).
- [24] B. Wang and K. Huang, Shaping the radiation pattern with mu and epsilon-near-zero metamaterials, *Prog. Electromagn. Res.* **106**, 107 (2010).
- [25] A. Alù and N. Engheta, Dielectric sensing in ϵ -near-zero narrow waveguide channels, *Phys. Rev. B* **78**, 045102 (2008).
- [26] N. Kinsey, C. DeVault, J. Kim, M. Ferrera, V. M. Shalaev, and A. Boltasseva, Epsilon-near-zero Al-doped ZnO for ultrafast switching at telecom wavelengths, *Optica* **2**, 616 (2015).
- [27] Z. Chai, X. Hu, F. Wang, C. Li, Y. Ao, Y. Wu, K. Shi, H. Yang, and Q. Gong, Ultrafast on-chip remotely-triggered all-optical switching based on epsilon-near-zero nanocomposites, *Laser Photonics Rev.* **11**, 1700042 (2017).
- [28] M. A. Vincenti, D. de Ceglia, A. Ciattoni, and M. Scalora, Singularity-driven second- and third-harmonic generation at ϵ -near-zero crossing points, *Phys. Rev. A* **84**, 063826 (2011).
- [29] G. V. Naik, V. M. Shalaev, and A. Boltasseva, Alternative plasmonic materials: Beyond gold and silver, *Adv. Mater.* **25**, 3264 (2013).
- [30] Z. Lu, W. Zhao, and K. Shi, Ultracompact electroabsorption modulators based on tunable epsilon-near-zero-slot waveguides, *IEEE Photonics J.* **4**, 735 (2012).
- [31] A. Anopchenko, S. Gurung, L. Tao, C. Arndt, and H. W. H. Lee, Atomic layer deposition of ultra-thin and smooth al-doped zno for zero-index photonics, *Mater. Res. Express* **5**, 014012 (2018).
- [32] See Supplemental Material at <http://link.aps.org/supplemental/10.1103/PhysRevApplied.12.054021> for the detailed discussions about model setup, collection efficiency, far-field emission patterns, comparison of ENZ film with gold and silver films, and experimental details including sample fabrication and measurement. R. Carminati, A. Cazé, D. Cao, F. Peragut, V. Krachmalnicoff, R. Pierrat, and Y. De Wilde, Electromagnetic density of states in complex plasmonic systems, *Surf. Sci. Rep.* **70**, 1 (2015); Y. Chen, T. R. Nielsen, N. Gregersen, P. Lodahl, and J. Mørk, Finite-element modeling of spontaneous emission of a quantum emitter at nanoscale proximity to plasmonic waveguides, *Phys. Rev. B* **81**, 125431 (2010); C. Ciraci, A. Rose, C. Argyropoulos, and D. R. Smith, Numerical studies of the modification of photodynamic processes by film-coupled plasmonic nanoparticles, *J. Opt. Soc. Am. B* **31**, 2601 (2014); J. D. Jackson, *Classical Electrodynamics* (Wiley, 1999).
- [33] H. J. Lezec, A. Degiron, E. Devaux, R. A. Linke, L. Martin-Moreno, F. J. Garcia-Vidal, and T. W. Ebbesen, Beaming light from a subwavelength aperture, *Science* **297**, 820 (2002).
- [34] L. Li, E. H. Chen, J. Zheng, S. L. Mouradian, F. Dolde, T. Schroder, S. Karaveli, M. L. Markham, D. J. Twitchen, and D. Englund, Efficient photon collection from a nitrogen vacancy center in a circular bullseye grating, *Nano Lett.* **15**, 1493 (2015).
- [35] E. Moreau, I. Robert, J. M. Gérard, I. Abram, L. Manin, and V. Thierry-Mieg, Single-mode solid-state single photon source based on isolated quantum dots in pillar microcavities, *Appl. Phys. Lett.* **79**, 2865 (2001).
- [36] T. Heindel, C. Schneider, M. Lermer, S. H. Kwon, T. Braun, S. Reitzenstein, S. Höfling, M. Kamp, and A. Forchel, Electrically driven quantum dot-micropillar single photon source with 34% overall efficiency, *Appl. Phys. Lett.* **96**, 011107 (2010).
- [37] K. G. Lee, X. W. Chen, H. Eglhidi, P. Kukura, R. Lettow, A. Renn, V. Sandoghdar, and S. Götzinger, A planar dielectric antenna for directional single-photon emission and near-unity collection efficiency, *Nat. Photon.* **5**, 166 (2011).
- [38] R. Maas, J. Parsons, N. Engheta, and A. Polman, Experimental realization of an epsilon-near-zero metamaterial at visible wavelengths, *Nat. Photon.* **7**, 907 (2013).
- [39] M. W. Doherty, N. B. Manson, P. Delaney, F. Jelezko, J. Wrachtrup, and L. C. L. Hollenberg, The nitrogen-vacancy colour centre in diamond, *Phys. Rep.-Rev. Sec. Phys. Lett.* **528**, 1 (2013).
- [40] A. Ugur, S. Kremling, F. Hatami, S. Hofling, L. Worschech, A. Forchel, and W. T. Masselink, Single-photon emitters based on epitaxial isolated InP/InGaP quantum dots, *Appl. Phys. Lett.* **100**, 023116 (2012).
- [41] E. Neu, D. Steinmetz, J. Riedrich-Möller, S. Gsell, M. Fischer, M. Schreck, and C. Becher, Single photon emission from silicon-vacancy colour centres in chemical vapour deposition nano-diamonds on iridium, *New J. Phys.* **13**, 025012 (2011).